Catalysis Science & Technology

Accepted Manuscript

ROYAL SOCIETY OF CHEMISTRY

www.rsc.org/catalysis

Cite this: DOI: 10.1039/c0xx00000x

www.rsc.org/xxxxxx

ARTICLE TYPE

CdS quantum dots and tungsten carbide supported on anatase-rutile composite TiO_2 for highly efficient visible-light-driven photocatalytic H_2 evolution from water

Yun-xiang Pan,[a,c] Tianhua Zhou,[a,b] Jianyu Han,[a] Jindui Hong,[a] Yabo Wang,[a] Wei Zhang*[a,d] and Rong Xu*[a,b]

Received (in XXX, XXX) Xth XXXXXXXXX 20XX, Accepted Xth XXXXXXXXX 20XX
DOI: 10.1039/b000000x

Developing efficient photocatalysts with noble-metal-free co-catalysts for the visible-light-driven photocatalytic H_2 evolution from water is appealing yet remains challenging. Herein, by supporting CdS QDs with diameters smaller than 5 nm and tungsten carbide (WC) on TiO_2, a CdS/WC/TiO_2 photocatalyst was fabricated for the visible-light-driven photocatalytic H_2 evolution from aqueous solution containing lactic acid as the electron donor. The optimal H_2 evolution rate on CdS/WC/TiO_2 (624.9 μmol h^{-1}) is comparable to the H_2 evolution rate on CdS/Pt/TiO_2 (636.2 μmol h^{-1}), indicating that WC is a good candidate to substitute Pt as the co-catalyst. Formation of an anatase-rutile composite TiO_2 with a rutile content of 68.7% makes great contribution to the efficient H_2 evolution on CdS/WC/TiO_2. The rutile-anatase composite TiO_2 promotes the separation of the photogenerated electron-hole pairs, and thereby benefits the efficient H_2 evolution reaction. The present work is expected to be helpful for designing efficient noble-metal-free photocatalysts for H_2 evolution from the visible-light-driven photocatalytic water splitting.

Introduction

H_2 production from photocatalytic water splitting by using solar light is promising for solving the energy and environmental crises facing mankind.[1-3] Cadmium sulfide (CdS) has been widely used as the photocatalyst for H_2 production from the photocatalytic water splitting, due to its tunable morphology, unique electronic and optical properties, adjustable band gaps as well as good response to visible light which is the main part of solar light (44%).[4-9] However, one of the challenges in utilizing CdS is the limited separation efficiency of the photoinduced electron-hole pairs on CdS.[6-9] Using CdS quantum dots (CdS QDs) with diameters smaller than 5 nm can greatly promote the electron-hole separation, due to shorter transportation path, quantum-confinement effect and lower density of defects.[6,9] Incorporating CdS onto support materials, such as TiO_2, is another way to promote the electron-hole separation.[2-6] The support materials can accept and help transfer the electrons to reaction sites, thus achieving the improved electron-hole separation efficiency.[6-13]

Another challenge lies on the use of platinum (Pt) co-catalyst on CdS.[15] Pt co-catalyst can greatly improve the photocatalytic water splitting efficiency on CdS-based photocatalysts.[1,6,8,9,11-14] However, due to the limited abundance and high price, Pt is not suitable for large-scale applications.[15] It is highly desirable to develop Pt-free co-catalysts. Transition metal carbides, such as tungsten carbide (WC), have been explored as the co-catalysts for H_2 production from the photocatalytic water splitting.[15-18] For example, the WC/CdS photocatalyst with WC as the co-catalyst or active sites exhibited a H_2 production rate of about 200 μmol h^{-1} from the visible-light-driven photocatalytic water splitting.[16] In transition metal carbides, the electronic structure of the host transition metal is modified by the inclusion of carbon interstitial atoms *via* charge transfer processes or/and structural modification.[15,17] Such modification in electronic structure makes transition metal carbides to exhibit similar properties as noble metals.[15,17] This indicates that transition metal carbides could be good candidates as co-catalysts in H_2 production from photocatalytic water splitting. Nonetheless, the activity of the photocatalysts with transition metal carbides as co-catalysts is still too low and requires further improvement for large-scale applications.

In the present work, a CdS/WC/TiO_2 composite photocatalyst was fabricated by supporting CdS QDs with diameters smaller than 5 nm and WC on TiO_2. The optimal H_2 evolution rate on CdS/WC/TiO_2 is as high as 624.9 μmol h^{-1}, which is comparable to that on CdS/Pt/TiO_2 (636.2 μmol h^{-1}), under visible light irradiation (λ > 420 nm) from water containing lactic acid as hole scavengers. The use of CdS QDs and formation of the anatase-rutile composite TiO_2 with suitable phase composition could be the key factors for the high H_2 evolution rate on CdS/WC/TiO_2.

Experimental

Sample preparation

CdS QDs used in the present work have an average diameter smaller than 5 nm and are water-soluble, and its synthesis

procedure has been described in detail in our previous work.[6,9] Fig. S1 in the supporting information shows a transmission electron microscopy (TEM) image of the CdS QDs.

Before loading CdS QDs, TiO_2-supported WC (WC/TiO_2) with a Ti/W molar ratio of 10/1 was synthesized through the following steps. Firstly, 250 mg of tungsten chloride (WCl_6, Alfa Aesar, purity ≥99.9%) was dissolved in ethanol (20 mL) to form a mixture. Then 500 mg of TiO_2 (P25, Alfa Aesar) was dispersed in the mixture, followed by stirring for 12 h. The as-obtained sample was centrifuged to get a precipitate which was dried at 60 °C for 12 h. After drying, the sample was calcined at 800 °C for 4 h in N_2 with a heating rate of 5 °C min^{-1}.

Loading of CdS QDs on WC/TiO_2 proceeded in 200 mL of aqueous solution containing 20 vol% lactic acid as the sacrificial reagent. WC/TiO_2 (30 mg) and CdS QDs (40 mg) were added into the solution under ultrasonication for 2 h. The mixture was then divided into two parts. One part (100 mL) was centrifuged to collect the solid sample which was washed by ethanol and deionized water for several times and subsequently dried in a vacuum freeze drier for further characterizations. The other part (100 mL) was used for photocatalytic H_2 evolution reaction under visible light.

Using the same procedure as $CdS/WC/TiO_2$, CdS/TiO_2 without WC, $CdS/WC/Al_2O_3$, $CdS/WC/SiO_2$, $CdS/WC/ZnO$, $CdS/WC/CeO_2$, $CdS/WC/ZrO_2$ and CdS/WC/MgO were also prepared. For comparison, commercial CdS (Sigma-Aldrich, purity: 99.999%) was also loaded on WC/TiO_2 by the same procedure, and the obtained sample was named as $CdS(C)/WC/TiO_2$. To prepare $CdS/Pt/TiO_2$, Pt was first deposited on TiO_2 according to the procedure reported in our previous work.[9] TiO_2 (100 mg) was impregnated with an aqueous solution (2.0 mL) of H_2PtCl_6 containing 2.0 mg Pt for 12 h under gentle stirring to form a mixture. $NaBH_4$ solution (0.1 M, 0.5 mL) was then added to the mixture which was kept under stirring for 2 h. The resultant sample was centrifuged and washed with ethanol and deionized water for several times, followed by drying in a vacuum freeze drier. Loading of CdS QDs on Pt/TiO_2 proceeded in the reaction solution containing 20 vol% lactic acid (100 mL) to which 15 mg of Pt/TiO_2 and a certain amount of CdS QDs were added and stirred for 2 h.

Characterization

Fourier transformation infrared (FTIR) spectra were recorded on a Digilab FTS 3100 FTIR using a standard KBr disk technique, with a 4 cm^{-1} resolution. The morphological features of the samples were observed on a field emission scanning electron microscope (FESEM, JEOL JSM 6700F). Nitrogen absorption-desorption measurement was conducted at 77.35 K on a Quantachrome Autosorb-6B apparatus to measure the Brunauer-Emmett-Teller (BET) surface areas. The crystallographic properties of the samples were analyzed by X-ray diffraction (XRD) patterns on a X-ray diffractometer (Bruker AXS D8, Cu Ka, l = 1.5406 Å, 40 kV and 20 mA). TEM observations of the samples, including energy dispersion X-ray spectroscopy (EDX) and elemental mapping, were performed on a JEOL JEM 2100F with a beam energy of 200 kV. Raman spectra were obtained on Jobin-Yvon LabRam HR800, using an Ar ion laser with a wavelength of 514 nm. UV-visible diffuse reflectance spectra were obtained using a UV-visible spectrophotometer (UV-2450, Shimadzu). The concentration of leached Cd ions during the photoreaction was determined by inductive coupled plasma optical emission spectrometer (ICP-OES) on an Agilent 7700x. X-ray photoelectron spectra (XPS) were obtained on an ESCALab MKII X-ray photoelectron spectrometer using Mg Kα radiation as the excitation source. Photoluminescence (PL) spectra were collected on a Jobin Yvon Fluorolog 3-TAU luminescence spectrometer (Jobin Yvon Instruments Co., Ltd., France).

Photoelectrochemical measurements were conducted on a CHI660C electrochemical workstation using a three-electrode cell with Pt plate as the counter electrode, saturated calomel electrode (SCE) as the reference electrode, and $WC/CdS/TiO_2$ coated on indium-tin-oxide (ITO) as the working electrode. The light source was a 300 W Xenon lamp with a cut-off filter (λ > 420 nm). $WC/CdS/TiO_2$ (1 mg) was dispersed in ethanol (1 mL) containing 0.05 wt% Naphthol followed by ultrasonication. The suspension was then deposited onto ITO, and dried at room temperature first and then at 60 ^oC for 1 h. The photocurrent was recorded in 0.25 M Na_2SO_4 aqueous solution containing 20 vol% lactic acid with a constant potential of 0.35 V versus SCE. The area irradiated was set at 0.25 cm^2.

Photoreaction

The H_2 production from the visible-light-driven water reduction was conducted in a closed gas circulation evacuation system fitted with a top window Pyrexcell with a total volume of 300 mL. The reaction solution with a volume of 100 mL containing different amounts of photocatalyst components and 20 vol% lactic acid was placed in the cell. The pH of the solution was measured to be 5.5. Before reaction, the system was evacuated and refilled with argon for several times to remove the air inside. The reaction was carried out using a 300 W Xenon lamp equipped with a cut-off filter (λ > 420 nm). The temperature of the photoreaction cell was kept at about 20°C by using cooling water. The H_2 produced was analyzed by online gas chromatography (Agilent 6890N, TCD detector) with a H_2 calibration curve obtained before the measurement using high purity H_2 (Air Liquid, 99.99%). The light irradiation time in each run was 6 h for activity measurement and the average H_2 production rate within 6 h was calculated and plotted. The QE value was measured under the same reaction conditions during the first 2 h of photoreaction. The lamp was equipped with band pass interference filters (Newport, center wavelength at 420, 440, 460, 480, 500 and 520 nm, band width 10 nm). The number of photons from the radiation source was measured using a silicon photodiode (13 DAS 005, MELLES GRIOT) connected to a broad band power/energy meter (13 PEM 001, MELLES GRIOT). The measured number of photons in 2 h was 204, 220, 326, 183, 413, and 459 μmol with the filter centered at 420, 440, 460, 480, 500 and 520 nm, respectively. QE was calculated by the following function:

$$QE = \frac{2\times(\text{the number of evolved } H_2 \text{ molecules})}{\text{the number of incident photons}} \times 100\%$$

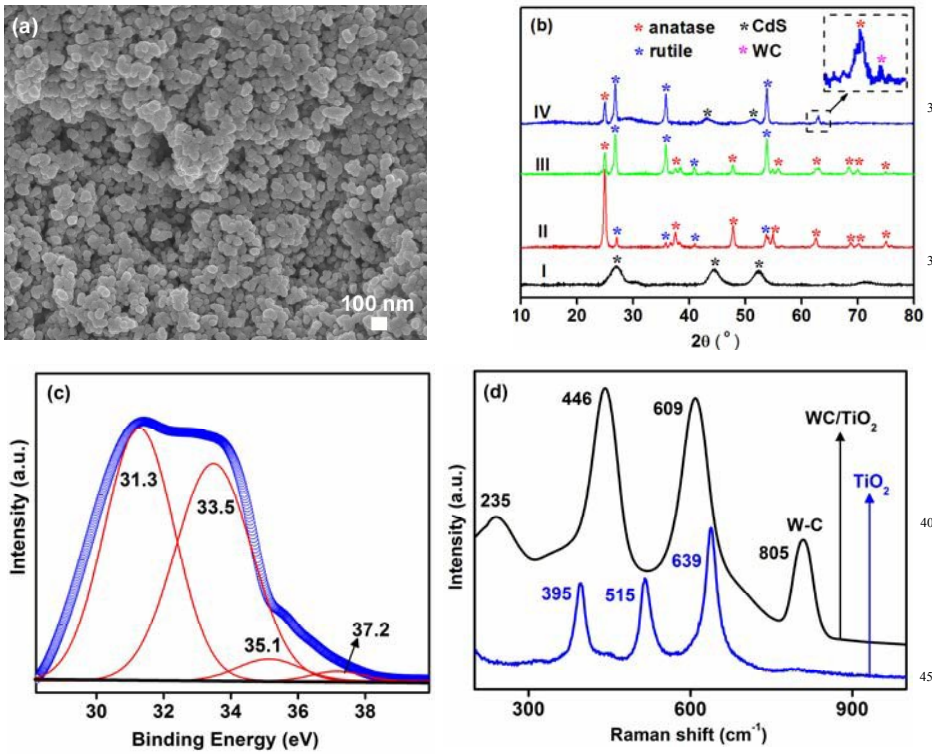

Fig. 1 (a) SEM image of WC/TiO_2. (b) XRD patterns of CdS QDs (I), pristine TiO_2 (II), WC/TiO_2 (III) and $CdS/WC/TiO_2$ prepared with 20 mg of CdS QDs and 15 mg of WC/TiO_2 (IV). (c) W_{4f} XPS spectrum of WC/TiO_2. (d) Raman spectra of TiO_2 and WC/TiO_2. WC/TiO_2 was obtained by calcination at 800 °C with a Ti/W molar ratio of 10/1.

Results and discussion

As proposed by Joo *et al.*[19] and Ryu *et al.*,[20] the following two reactions occur between WCl_6 and ethanol:

$$xWCl_6 + xCH_3CH_2OH \rightarrow WCl_{6-x}(OC_2H_5)_x + xHCl$$

$$WCl_{6-x}(OC_2H_5)_x + (6-x)CH_3CH_2OH \rightarrow W(OC_2H_5)_6 + (6-x)HCl$$

Therefore, the preparation of WC/TiO_2 is proposed to proceed *via* the following steps. WCl_6 first reacts with ethanol to form $W(OC_2H_5)_6$ which is then deposited on the surface of TiO_2 to generate $W(OC_2H_5)_6/TiO_2$. Subsequent calcination of $W(OC_2H_5)_6/TiO_2$ leads to the formation of WC/TiO_2. FTIR analysis was conducted for TiO_2 and $W(OC_2H_5)_6/TiO_2$ before calcination. As shown in Fig. S2 in the supporting information, peaks at 3420, 1630 and 500 cm^{-1} are present on the FTIR spectra of both TiO_2 and $W(OC_2H_5)_6/TiO_2$. The peaks at 3420 and 1630 cm^{-1} correspond to the stretching vibration modes of water or hydroxyl groups.[21] The peak at 500 cm^{-1} is attributed to the vibration mode of Ti-O-Ti bonds.[21] The fingerprint at about 2930 cm^{-1} on the spectrum of $W(OC_2H_5)_6/TiO_2$ is assigned to the $\upsilon_{as}(CH_3)$ vibrational mode of the OC_2H_5 group.[22]

As shown in the SEM image (Fig. 1a), the sample WC/TiO_2 consists of particles of with an average diameter of around 100 nm. The BET specific surface area of WC/TiO_2 was measured to be 44.7 $m^2\ g^{-1}$. As shown in Fig. 1b, the characteristic peaks of both anatase and rutile TiO_2 can be observed on the XRD patterns of the pristine TiO_2 and WC/TiO_2. The XRD peaks of anatase TiO_2 appear at 25.2°, 37.8°, 48.0°, 55.1°, 62.1°, 68.8°, 70.3° and 75.0° (PDF#21-1276), while those of rutile TiO_2 at 27.4°, 36.1°, 41.2° and 54.3° (PDF#21-1276). As compared with the pristine TiO_2, the anatase TiO_2 peaks become weaker whereas the rutile TiO_2 peaks get stronger in WC/TiO_2 and $CdS/WC/TiO_2$. The content of the rutile TiO_2 in the samples was estimated by the following equation: [21]

$$\text{Rutile Content} = \frac{1}{(1+0.8\frac{I_A}{I_R})} \times 100\%$$

where I_A and I_R are the intensity of the XRD peak of anatase and rutile TiO_2 at 25.1° and 27.3°, respectively. The rutile content in WC/TiO_2 is about 68.7%, much higher than that in the pristine TiO_2 (about 20%). This implies that heat treatment of WC/TiO_2 induces a significant change in the ratio between the anatase and rutile phases in TiO_2. It has been reported that calcination is the key factor affecting the phase composition of TiO_2, and a higher calcination temperature results in a higher content of rutile phase.[21,23] There is a small peak at 64.0° on the XRD pattern of WC/TiO_2, which is assigned to the (110) plane of cubic WC (PDF#20-1316). The low intensity can be attributed to its low percentage and small domain size.

XPS analysis was used to further detect the presence of WC on the surface of TiO_2. The spectrum of W_{4f} can be deconvoluted to four peaks (Fig. 1c). The two major peaks at 31.3 and 33.5 eV can be attributed to $W_{4f7/2}$ and $W_{4f5/2}$ of WC.[24-26] The minor peaks at 35.1 and 37.2 eV are due to partially oxidized tungsten.[24,26] WC could interact with the TiO_2 support through W-O bonds, causing some tungsten in higher oxidation state. Fig. 1d plots the Raman spectra of the pristine TiO_2 and WC/TiO_2. The characteristic Raman peaks of anatase TiO_2, locating at 395, 515 and 639 cm^{-1}, appear on the pristine TiO_2.[27] There are four peaks, located at 235, 446, 609 and 805 cm^{-1}, on the Raman spectrum of WC/TiO_2. The first three peaks correspond to rutile TiO_2,[27] while the last peak at 805 cm^{-1} is resulted from the stretching mode of W-C bond in WC.[28]

On the XRD pattern of $CdS/WC/TiO_2$ (Fig. 1b), besides the peaks assigned to TiO_2 and WC, there are also two diffraction peaks at 44.0° and 52.1°, which match well with the (220) and (311) diffraction of the standard cubic CdS (PDF#47-1179). The lattice fringes with d = 0.25 and 0.35 nm are observed in the HRTEM image of $CdS/WC/TiO_2$ (Fig. 2a), and are attributed to the WC(100) and CdS(111) planes, respectively. The EDX and elemental mapping results (Figs. 2b-2d) confirm the presence of W, Ti, Cd and S on $CdS/WC/TiO_2$. As shown in the UV-visible DRS results in Fig. 2e, after coating of CdS QDs and WC, the samples display significantly enhanced absorption of visible light compared to the pristine TiO_2.

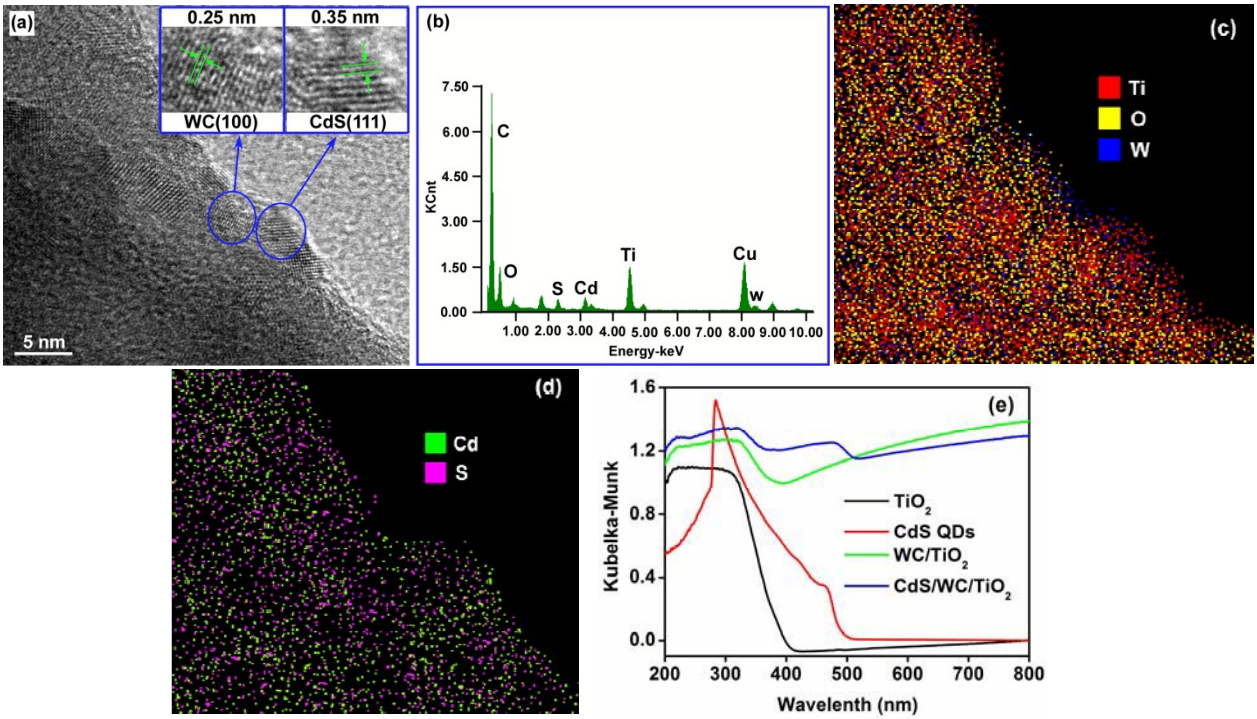

Fig. 2 (a) HRTEM image, (b) EDX and (c, d) elemental mapping images of CdS/WC/TiO_2. (e) UV-visible DRS results of TiO_2, CdS QDs, WC/TiO_2 and CdS/WC/TiO_2. CdS/WC/TiO_2 was prepared with 20 mg of CdS QDs and 15 mg of WC/TiO_2 which was obtained by calcination at 800 °C with a Ti/W molar ratio of 10/1.

Fig. 3 displays the activities of the photocatalysts and control samples for H_2 evolution from the aqueous solution containing lactic acid as hole scavengers under visible light irradiation ($\lambda >$ 420 nm). The time-course of H_2 evolution are displayed in Fig. S3. No appreciable amount of H_2 was generated without either irradiation or photocatalyst, implying the evolution of H_2 is from the photocatalytic reaction. A factor affecting the H_2 evolution rate on CdS/WC/TiO_2 is the mass ratio between CdS QDs and WC/TiO_2, as illustrated in Fig. 3a. By fixing the amount of CdS QDs (20 mg), the H_2 evolution increases from 68.0 μmol h^{-1} to 622.1 μmol h^{-1}, by increasing the amount of WC/TiO_2 from 0 to 15 mg. As WC acts as the co-catalyst, a higher concentration of WC/TiO_2 allows a more efficient charge transfer from CdS to WC, resulting in a higher H_2 evolution rate. The H_2 evolution rate decreases when the mass of WC/TiO_2 is greater than 15 mg in 100 mL of reaction solution. Aggregation of WC/TiO_2 particles or the self-filtering effect may occur when the concentration of WC/TiO_2 exceeds a certain level which has a negative effect on the H_2 evolution. Fig. 3b shows the H_2 evolution rates on CdS/WC/TiO_2 with different initial molar ratio of Ti/W when preparing WC/TiO_2, ranging from 10/0.2 to 10/3. Without WC, the H_2 evolution rate on CdS/TiO_2 is as low as 28.1 μmol h^{-1}. This suggests that WC acts as the co-catalyst for H_2 evolution. The photocatalytic activity reaches the optimum at a Ti/W molar ratio of 10/1.

Fig. 3c plots the H_2 evolution rate on CdS/WC/TiO_2 as a function of the calcination temperature used when preparing WC/TiO_2 ranging from 500 to 1000 °C. The optimal calcination temperature is 800 °C at which the H_2 evolution rate is 624.9 μmol h^{-1}. The considerable enhancement in the H_2 evolution rate could be due to the rutile-anatase phase junction formed in TiO_2 which will be discussed shortly. In addition, TiO_2 was substituted by Al_2O_3, SiO_2, ZnO, CeO_2, ZrO_2 and MgO to construct a series of CdS/WC/oxide photocatalysts. As shown in Fig. 3d, the activities of CdS/WC/Al_2O_3, CdS/WC/SiO_2, CdS/WC/ZnO, CdS/WC/CeO_2, CdS/WC/ZrO_2 and CdS/WC/MgO are all lower than that of CdS/WC/TiO_2. It is worth noting that although charge transfer between CdS QDs and the wide band gapped metal oxides including Al_2O_3, SiO_2, CeO_2, ZrO and MgO under visible light is not possible, they could still play a promotional effect on charge separation. As revealed in our previous work,[9] the surface defects (such as oxygen defects) on metal oxide may play a key role in trapping charge carriers, resulting in efficient charge localization and enhanced photocatalytic activity. CdS sample from commercial supply with an average particle size of about 1 μm was also used for comparison.[29] The H_2 evolution rate on CdS(C)/WC/TiO_2 is 167.5 μmol h^{-1} (Fig. 3c), which is much lower than those obtained with CdS QDs. It is believed that well-dispersed CdS QDs on the surface of TiO_2 can lead to favorable interaction with TiO_2 and WC co-catalyst. Such spacial arrangement should be the important factor towards much improved activities, in addition to the quantum size confinement effect of CdS QDs.[9]

The activity of CdS/WC/TiO_2 was compared with that of CdS/Pt/TiO_2. As shown in Fig. S4, by varying the mass ratio between CdS QDs and Pt/TiO_2 and varying the loading amount of Pt, an optimal H_2 evolution rate of 636.2 μmol h^{-1} was obtained on CdS/Pt/TiO_2. The H_2 evolution rate on CdS/Pt/TiO_2 is close to that on CdS/WC/TiO_2 (624.9 μmol h^{-1}). In addition, as listed in Table S1, the activity of CdS/WC/TiO_2 is comparable or better than those of the CdS/Pt/oxide systems reported in literatures.[9,11,12,30-32] As such, WC is a promising candidate to substitute Pt as the co-catalyst for photocatalytic H_2 production under visible light.

Stability of CdS/WC/TiO_2 was examined in five consecutive runs with each run of 12 h (Fig. 3e). There is about 14% decrease in total amount of H_2 produced after five runs, from 6593 μmol in the first run to 5670 μmol in the fifth run. The decrease of the H_2 amount may due to the dissolution of CdS QDs during the photocatalytic reaction in acidic environment. ICP measurements indicate that about 10% of CdS QDs is dissolved to Cd ions into the reaction solution after the stability test. The QE of

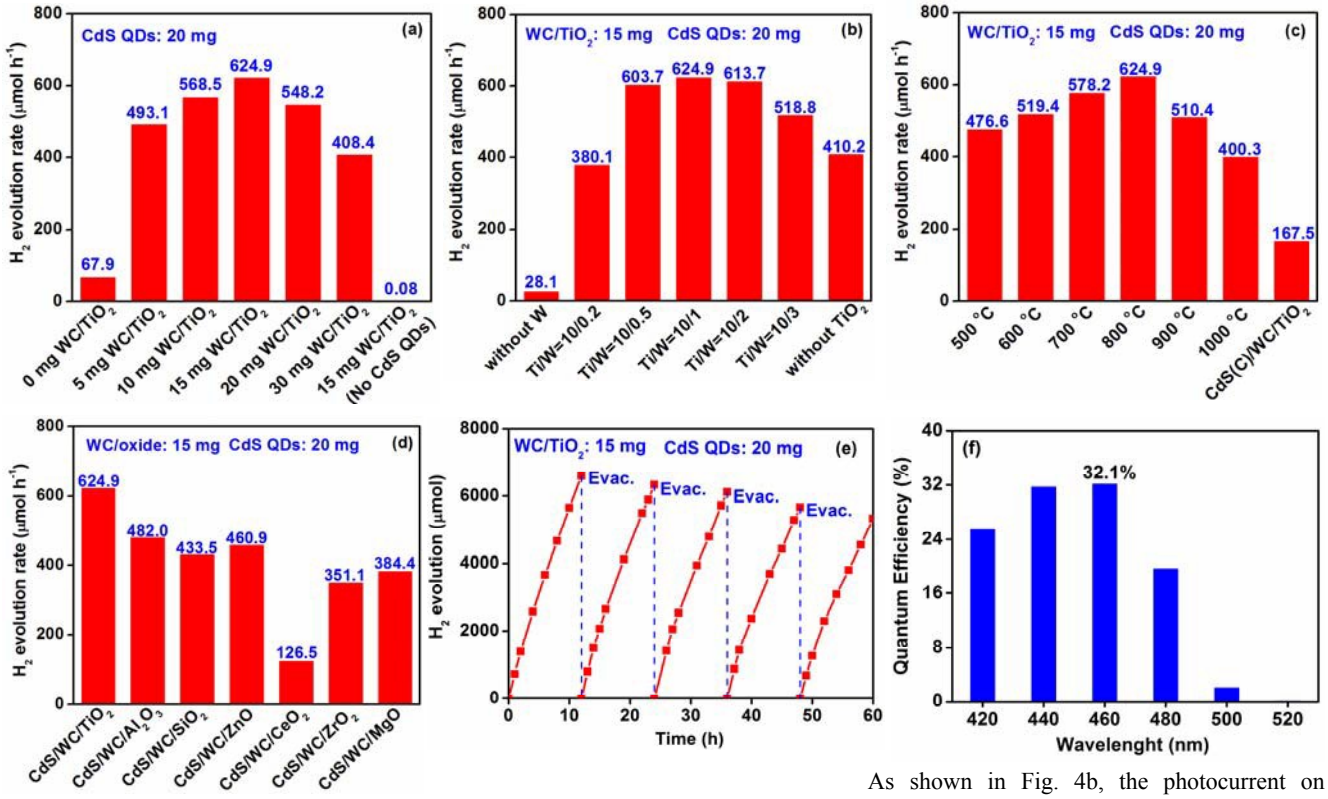

Fig. 3 (a) H_2 evolution rate with different amount of WC/TiO_2 (calcined at 800 °C, Ti/W molar ratio: 10/1) by fixing the amount of CdS QDs at 20 mg. (b) H_2 evolution rate with different molar ratio of Ti/W by fixing the amounts of WC/TiO_2 (calcined at 800 °C) and CdS QDs at 15 and 20 mg, respectively. (c) H_2 evolution rate with different calcination temperature by fixing the amounts of WC/TiO_2 (Ti/W molar ratio: 10/1) and CdS QDs at 15 and 20 mg, respectively. (d) H_2 evolution rate on photocatalysts with different metal oxide supports by fixing the amount of WC/oxide (15 mg) and CdS QDs (20 mg). (e) Stability of CdS/WC/TiO_2. (f) QE values under photons with different wavelengths on CdS/WC/TiO_2. CdS/WC/TiO_2 used for stability and QE measurements was prepared with 20 mg of CdS QDs and 15 of mg WC/TiO_2 which was obtained by calcination at 800 °C with a Ti/W molar ratio of 10/1. Reaction conditions: 100 mL aqueous solution with 20 vol% lactic acid, 300 W Xe lamp (λ > 420 nm).

CdS/WC/TiO_2 increases with the increasing wavelength of the monochromatic light from 420 to 460 nm, and decreases with the wavelength larger than 460 nm (Fig. 3f). The highest QE of CdS/WC/TiO_2 is present at 460 nm, with a value of 32.1%.

As shown in Fig. 3a, there is almost no H_2 produced on WC/TiO_2, due to the absence of CdS QDs which is responsible for harvesting visible light. Without WC which serves as the co-catalysts or active sites for the photocatalytic water splitting to H_2, the H_2 evolution rate on CdS/TiO_2 is only 28.1 μmol h^{-1} (Fig. 3b), much lower than that on CdS/WC/TiO_2. As shown in Fig. 3b, the H_2 evolution rate on CdS/WC/TiO_2 (624.9 μmol h^{-1}) is higher than that on the WC/CdS without TiO_2 (410.2 μmol h^{-1}). Such activity improvement in the presence of TiO_2 could result from the higher separation efficiency of the photogenerated electron-hole pairs in the presence of TiO_2, as reflected by the PL spectra shown in Fig. 4a. The pure CdS QDs shows a higher PL peak at about 490 nm, which is induced by the recombination of the photogenerated electron-hole pairs in the pure CdS QDs.[9,33] As compared with the pure CdS QDs, the PL is quenched significantly on CdS/WC/TiO_2, indicating an efficient separation of the photogenerated electron-hole pairs. Photocurrent measurement is another method to detect the separation efficiency of the photogenerated electron-hole pairs.[9,34] A higher photocurrent suggests a more efficient electron-hole separation. As shown in Fig. 4b, the photocurrent on CdS/WC/TiO_2 is much higher than that on the pure CdS QDs. Therefore, the separation efficiency of the photogenerated electron-hole pairs on CdS/WC/TiO_2 is significantly improved. Fig. 4c plots the band alignment of the pure CdS QDs, anatase TiO_2 and rutile TiO_2.[9,35] The conduction band (CB) of CdS QDs is higher than those of both anatase and rutile TiO_2. This can promote the transfer of the photoinduced electrons from the CB of CdS QDs to the CB of TiO_2, which benefits the separation of the photogenerated electron-hole pairs. An efficient electron-hole separation will lead to more photogenerated electrons participating in the photocatalytic water splitting, and thereby a higher H_2 evolution rate.

Formation of the anatase-rutile composite TiO_2 could also make great contribution to the efficient separation of the photogenerated electron-hole pairs, and thereby to the increased

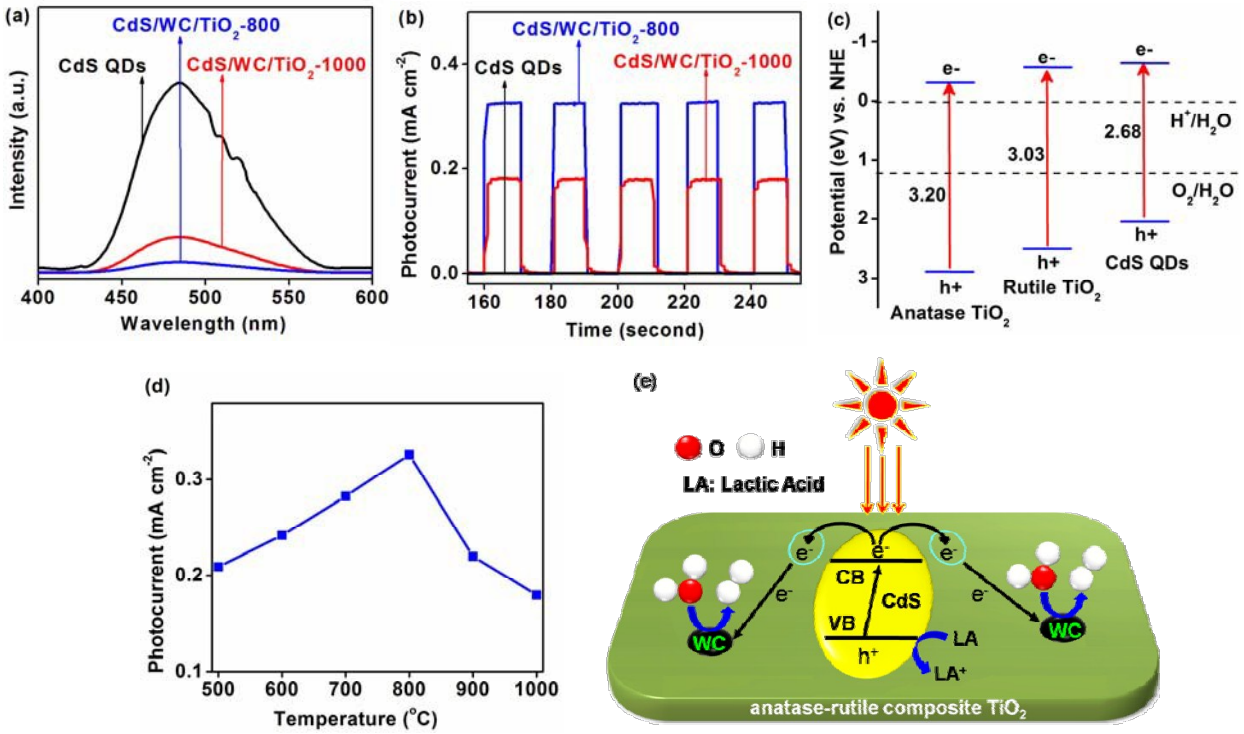

Fig. 4 (a) PL spectra of the pure CdS QDs, CdS/WC/TiO_2-800 and CdS/WC/TiO_2-1000 at excitation wavelength of 365 nm. (b) Transient photocurrent response of pure CdS QDs, CdS/WC/TiO_2-800 and CdS/WC/TiO_2-1000 in 0.2 M Na_2SO_4 aqueous solution containing 20 vol% lactic acid under visible light irradiation ($\lambda > 420$ nm). (c) Band alignment of the pure CdS QDs, anatase TiO_2 and rutile TiO_2. (d) Transient photocurrent as a function of the calcination temperature used for preparing WC/TiO_2. (e) Possible mechanism of the visible-light-driven photocatalytic H_2 production from water containing lactic acid (LA) as hole scavengers on CdS/WC/TiO_2. CB and VB label the conduction band and valence band, respectively. CdS/WC/TiO_2 was prepared with 20 mg of CdS QDs and 15 mg of WC/TiO_2 which was prepared with a Ti/W molar ratio of 10/1.

H_2 evolution rate, on CdS/WC/TiO_2. For determining the effect of the anatase-rutile composite TiO_2 on the separation of the photogenerated electron-hole pairs on CdS/WC/TiO_2, we compared the PL and photocurrent of the WC/CdS/TiO_2 with WC/TiO_2 calcined at 800 and 1000 °C. For clarity, the WC/TiO_2 calcined at 800 and 1000 °C are denoted by WC/TiO_2-800 and WC/TiO_2-1000, respectively. Fig. S5 shows the XRD patterns of WC/TiO_2 calcined at different temperatures. The content of the rutile TiO_2 in WC/TiO_2-800 and WC/TiO_2-1000 was calculated to be 68.7% and 100%, respectively. As shown in Fig. 4a, both CdS/WC/TiO_2-800 and CdS/WC/TiO_2-1000 exhibit quenched PL peaks as compared with the pure CdS QDs, with the quench on CdS/WC/TiO_2-800 more evident. As illustrated in Fig. 4b, both CdS/WC/TiO_2-800 and CdS/WC/TiO_2-1000 show enhanced photocurrent as compared with the pure CdS QDs, with the enhancement on CdS/WC/TiO_2-800 more significant. These results suggest that the electron-hole separation efficiency on CdS/WC/TiO_2-800 with an anatase-rutile composite TiO_2 is higher than that on CdS/WC/TiO_2-1000 with only rutile TiO_2. Since the specific surface areas of WC/TiO_2-800 and WC/TiO_2-1000 are very similar at 44.7 and 43.6 $m^2\ g^{-1}$, respectively, the compositional difference between the two samples is believed to be the main contributing factor for the charge separation efficiency and higher activity.

Fig. 4d displays the photocurrent of WC/CdS/TiO_2 as a function of calcination temperature used when preparing WC/TiO_2. The photocurrent becomes higher with an increased calcination temperature from 500 to 800 °C, and then decreases when the calcination temperature increases further to 900 and 1000 °C. Based on the XRD results shown in Fig. S5, the content of the rutile TiO_2 in the WC/TiO_2 calcined at 500 °C, 600 °C, 700 °C, 800 °C, 900 and 1000 °C are 15.1%, 20.2%, 60.7%, 68.7%, 96.3% and 100%, respectively. These results indicate that the separation efficiency of the photogenerated electron-hole pairs on CdS/WC/TiO_2 depends strongly on the anatase/rutile ratio, and the highest separation efficiency is obtained at a calcination temperature of 800 °C. This could be the origin for the higher H_2 evolution rate on CdS/WC/TiO_2 with WC/TiO_2 calcined at 800 °C than those on the other photocatalysts (Fig. 3c). In addition, the photocurrents of CdS/WC/Al_2O_3, CdS/WC/ZnO, CdS/WC/CeO_2 and CdS/WC/MgO under the same conditions as that of CdS/WC/TiO_2 were measured. As shown in Fig. S6 in the supporting information, the photocurrents of CdS/WC/Al_2O_3, CdS/WC/CeO_2 and CdS/WC/MgO are all much lower than that of CdS/WC/TiO_2, which could be caused by the wide band gaps of Al_2O_3, CeO_2 and MgO. The band gap of ZnO is close to that of TiO_2. However, the photocurrent of CdS/WC/ZnO is also lower than that of CdS/WC/TiO_2. These results further indicate the importance of the rutile-anatase composite TiO_2 for achieving the highly efficient separation of the photogenerated electron-hole pairs on CdS/WC/TiO_2.

On the basis of the above discussions, the possible mechanism of the H_2 evolution from the photocatalytic water splitting on CdS/WC/TiO_2 is proposed, as illustrated in Fig. 4e.

Visible light irradiation leads to the excitation of the electrons from the valance band (VB) to conduction band (CB) of the supported CdS QDs. The photogenerated electrons are then efficiently transferred to the supported WC *via* the anatase-rutile composite TiO_2 support. Finally, the electrons react with H_2O to form H_2 on the supported WC.

Conclusions

In this work, a CdS/WC/TiO_2 photocatalyst was fabricated by supporting CdS QDs with diameters smaller than 5 nm and WC on TiO_2, and was applied for visible-light-driven H_2 evolution from water containing lactic acid as a hole scavenger. The optimal H_2 evolution rate on CdS/WC/TiO_2 (624.9 μmol h^{-1}) is comparable to that on CdS/Pt/TiO_2 (636.2 μmol h^{-1}), indicating the potential of substituting the expensive Pt cocatalyst by WC for H_2 evolution. The H_2 evolution rate on CdS/WC/TiO_2 is higher than those on the photocatalyst with CdS QDs being replaced by commercial CdS, WC/CdS without TiO_2, and the photocatalysts with TiO_2 being substituted by Al_2O_3, SiO_2, ZnO, CeO_2, ZrO_2 and MgO. The use of CdS QDs and the formation of the anatase-rutile composite TiO_2 with an appropriate phase composition could be the keys for the higher H_2 evolution rate on CdS/WC/TiO_2. The rutile-anatase junction in TiO_2 promotes the separation of the photogenerated electron-hole pairs. This is favourable for a higher H_2 evolution rate. It is believed that the findings in this work are useful for designing efficient noble-metal-free photocatalysts for H_2 evolution under visible light.

Acknowledgments

This work was supported by National Environment Agency, Singapore under the Environment Technology Research Programme (ETRP) through Project no.: ETRP 1002 103, and Singapore National Research Foundation (NRF) through the Singapore-Berkeley Research Initiative for Sustainable Energy (SinBeRISE) CREATE Programme. The authors are thankful to H. Liu and Prof Y. Z. Huang from School of Materials Science and Engineering, NTU, for assisting TEM analysis.

Notes and references

[a] *School of Chemical & Biomedical Engineering, Nanyang Technological University, 62 Nanyang Drive,* Singapore 637459. Fax: (+65) 6794 7553. E-mail: rxu@ntu.edu.sg

[b] *SinBeRISE CREATE, National Research Foundation, CREATE Tower level 11, 1 Create Way, University Town, National University of Singapore, Singapore 138602*

[c] *School of Chemistry and Chemical Engineering, Hefei University of Technology, HeFei AnHui 230009, China*

[d] *School of Chemistry & Chemical Engineering, Shaanxi Normal University, Xi'an 710119, China. Email: zw@snnu.edu.cn*

†Electronic Supplementary Information (ESI) available: TEM image of CdS QDs; FTIR spectra; Activity data of CdS/Pt/TiO_2 and XRD partterns. See DOI: 10.1039/b000000x/

1 A. Kudo and Y. Miseki, *Chem. Soc. Rev.*, 2009, **38**, 253-278.
2 J. Xing, W. Q. Fang, H. J. Zhao and H. G. Yang, Chem. Asian J., 2012, 7, 642-657.
3 Y. Lan, Y. Lu and Z. Ren, Nano Energy, 2013, 2, 1031-1045.
4 T. Y. Zhai, X.S. Fang, L. Li, Y. Bando and D. Golberg, Nnaoscale, 2010, 2, 168-187.
5 H. Tada, M. Fujishima and H. Kobayashi, Chem. Soc. Rev., 2011, 40, 4232-4243.
6 Z. Fang, Y. Wang, J. Song, Y. Sun, J. Zhou, R. Xu and H. Duan, Nanoscale, 2013, 5, 9830-9838.
7 Y. K. Kim and H. Park, Energy Environ. Sci., 2011, 4, 685-694.
8 Q. Li, B. Guo, J. Yu, J. Ran, B. Zhang, H. Yan and J. R. Gong, J. Am. Chem. Soc., 2011, 133, 10878-10884.
9 Y. -X. Pan, H. Zhuang, J. Hong, Z. Fang, H. Liu, B. Liu, Y. Huang and R. Xu, ChemSusChem, 2014, 7, 2537-2544.
10 S. -W. Cao, Y. -P. Yuan, J. Fang, M. M. Shahjamali, F. Y. C. Boey, J. Barber, S. C. Joachim Loo and C. Xue, Int. J. Hydrogen Energy, 2013, 38, 1258-1266.
11 S. R. Lingampalli, U. K. Gautam and C. N. R. Rao, Energy Environ. Sci., 2013, 6, 3589.
12 J. S. Jang, S. H. Choi, H. G. Kim and J. S. Lee, J. Phys. Chem. C, 2008, 112, 17200-17205.
13 H. Park, Y. K. Kim and W. Choi, J. Phys. Chem. C, 2011, 115, 6141-6148.
14 J. H. Yang, D. G. Wang, H. X. Han and C. Li, Acc. Chem. Res., 2013, 46, 1900-1909.
15 W. F. Chen, J. T. Muckerman and E. Fujita, Chem. Commun., 2013, 49, 8896-8909.
16 J. S. Jang, D. J. Ham, N. Lakshminarasimhan, W. Y. Choi and J. S. Lee, Appl. Catal. A: General, 2008, 346, 149-154.
17 A. T. Garcia-Esparza, D. Cha, Y. W. Ou, J. Kubota, K. Domen and K. Takanabe, ChemSusChem, 2013, 6, 168-181.
18 J. Ran, J. Zhang, J. Yu, M. Jaroniec and S. Z. Qiao, Chem. Soc. Rev., 2014, 43, 7787-7812.
19 J. B. Joo, J. S. Kim, P. Kim and J. Yi, Mater. Lett., 2008, 62, 3497-3499.
20 H. -W. Ryu and K. -H. Park, J. Korean Phys. Soc., 2003, 42, L727-L730.
21 L. Zhang, M. S. Tse, O. K. Tan, Y. X. Wang and M. Han, J. Mater. Chem. A, 2013, 1, 4497.
22 J. J. Murcia, M. C. Hidalgo, J. A. Navío, J. Araña and J. M. Doña-Rodríguez, Appl. Catal. B: Environ., 2013, 142-143, 205-213.
23 J. Zhang, Q. Xu, Z. Feng, M. Li and C. Li, Angew. Chem. Int. Ed., 2008, 47, 1766-1769.
24 K. A. Beadle, R. Gupta, A. Mathew, J. G. Chen and B. G. Willis, Thin Solid Films, 2008, 516, 3847-3854.
25 J. B. Joo, J. S. Kim, P. Kim and J. Yi, Mater. Lett., 2008, 62, 3497-3499.
26 C. Moreno-Castilla, M. A. Alvarez-Merino, F. Carrasco-Marin and J. L. G. Fierro, Langmuir, 2001, 17, 1752–1756.
27 Y. Cai, B. Zhao, J. Wang and Z. Shao, J. Power Sources, 2014, 253, 80-89.
28 L. C. Agudelo-Morimitsu, J. De La Roche, D. Escobar, R. Ospina and E. Restrepo-Parra, Ceram. Int., 2013, 39, 7355-7365.
29 Y. Wang, Y. Wang and R. Xu, J. Phys. Chem. C, 2013, 117, 783-790.
30 X. Wang, G. Liu, Z. G. Chen, F. Li, L. Wang, G. Q. Lu and H. M. Cheng, Chem. Commun., 2009, 3452-3454.
31 D. Barpuzary, Z. Khan, N. Vinothkumar, M. De and M. Qureshi, J. Phys. Chem. C, 2012, 116, 150-156.
32 R. Marschall and L. Wang, Catal. Today, 2014, 225, 111-135.
33 J. Yang, H. Yan, X. Wang, F. Wen, Z. Wang, D. Fan, J. Shi and C. Li, J. Catal., 2012, 290, 151-157.
34 N. Zhang, M. -Q. Yang, Z. -R. Tang and Y. -J. Xu, J. Catal., 2013, 303, 60-69.
35 D. O. Scanlon, C. W. Dunnill, J. Buckeridge, S. A. Shevlin, A. J. Logsdail, S. M. Woodley, C. R. Catlow, M. J. Powell, R. G. Palgrave, I. P. Parkin, G. W. Watson, T. W. Keal, P. Sherwood, A. Walsh and A. A. Sokol, Nat. Mater., 2013, 12, 798-801.

Table of Content (TOC)

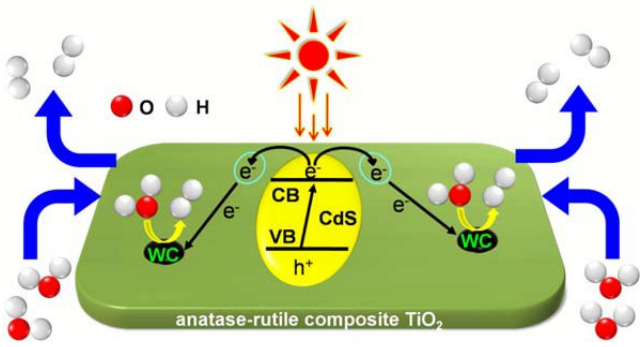

A noble-metal-free CdS/WC/TiO_2 photocatalyst with water-soluble CdS quantum dots (< 5nm) and anatase-rutile composite TiO_2 is highly efficient for H_2 evolution from the visible-light-driven photocatalytic water reduction.